Author 1:
John G. VanOsdol
National Energy Technology Center
3610 Collins Ferry Road
Morgantown WV 26507-0880
Email: jvanos@netl.doe.gov
Tel: (304) 285-5446
Fax: (304) 285-4403

Author 2:
Ta-Kuan Chiang
National Energy Technology Center
3610 Collins Ferry Road
Morgantown WV 26507-0880
Email: tchian@netl.doe.gov
Tel: (304) 285-4406
Fax: (304) 285-4403

Descriptive Title: A Fast Network Flow Model is used in conjunction with Measurements of Filter Permeability to calculate the Performance of Hot Gas Filters.

Keywords: Filtration, Permeability, Ceramic Barrier Filters, Gas Cleaning, Porous Medium, Clean Coal.

1.0   INTRODUCTION

Two different technologies that are being considered for generating electric power on a large scale by burning coal are Pressurized Fluid Bed Combustion (PFBC) systems and Integrated Gassification and Combined Cycle (IGCC) systems. Particulate emission regulations that have been proposed for future systems may require that these systems be fitted with large scale Hot Gas Clean-Up (HGCU) filtration systems that would remove the fine particulate matter from the hot gas streams that are generated by PFBC and IGCC systems. These hot gas filtration systems are geometrically and aerodynamically complex. They typically are constructed with large arrays of ceramic candle filter elements (CFE). The successful design of these systems require an accurate assessment of the rate at which mechanical energy of the gas flow is dissipated as it passes through the filter containment vessel and the individual candle filter elements that make up the system. Because the filtration medium is typically made of a porous ceramic material having open pore sizes that are much smaller than the dimensions of the containment vessel, the filtration medium is usually considered to be a permeable medium that follows Darcy's law. The permeability constant that is measured in the lab is considered to be a function of the filtration medium only and is usually assumed to apply equally to all the filters in the vessel as if the flow were divided evenly among all the filter elements. In general, the flow of gas through each individual CFE will depend not only on the geometrical characteristics of the filtration medium, but also on the local mean flows in the filter containment vessel that a particular filter element sees. The flow inside the CFE core, through the system manifolds, and inside the containment vessel itself will be coupled to the flow in the filter medium by various Reynolds number effects. For any given filter containment vessel, since the mean flows are different in different locations inside the vessel, the flow of gas through an individual CFE will adjust itself to accommodate the local mean flows that prevail in its general location. In some locations this adjustment will take place at High Reynolds numbers and in other locations this will occur at low Reynolds numbers. The analysis done here investigates the nature of this coupling.

2.0   LABORATORY ANALYSIS

Experimental Program

The NETL experimental facility is shown with its candle filter elements exposed in Figure (1). In this study they're were three different geometrical configurations tested in this facility. A schematic diagram of the various experimental configurations is shown in Figure (2). For each configuration the length of candle filter elements and the number of candle filter elements in the containment vessel was changed. For each configuration both virgin and conditioned candle filters were tested. The virgin filters used in these studies were filters that have never been exposed to flows that contain any particulates. The medium for the virgin filters was considered to be uniform. The conditioned filters were exposed for specified periods of time to particulate laden gas flows that were assumed to be uniformly loaded with particulate matter. There was no rigorous way of controlling this exposure so variations in the data could result. In the experimental test facility the inlet gas pressure, temperature, and flow rate could be independently controlled. These are shown on Table (1). The resulting system pressure drop was taken across the tube sheet that separates the vessel inlet to the outlet. These measurements are also shown on Table (1).

**Pressure drop occurs mainly upstream of the tube sheet.**

The ratio of the total system pressure drop to the dynamic pressure of the flow as it passes through the exit holes at the top of the filter elements into the clean side of the filter containment vessel is shown in Figure (3). If there were a substantial possibility of pressure recovery occurring in the system in any location on the clean side of the filter elements then this number would have to be less than 10. The data shows that in the majority of the test runs this ratio was well above 10. Some of the data shows values of this ratio greater than 1, but less than 10. This occurred for the cases where the system flow rate was uncharacteristically high. For these particular cases there could be a possibility of some small pressure recovery from the flow issuing out of the exit holes of the individual filter elements if this flow impinged on the top surface of the filter containment vessel. In the analysis it is assumed that this did not occur.

Pressure drop seems to follow Darcy's Law.

The system pressure drop for both virgin and conditioned filters having the same geometrical configuration inside the filter vessel is shown in Figure (4). The configuration shown was the 3 filter elements of 1.5 meter in length. Plotted on logarithmic axis the data shows a slope of 1 for both the virgin and the conditioned filters. Looking at this alone might tempt one in using Darcy's law to model the performance of the filters in this system. The assumption would be that as the filter media becomes loaded with particulate matter the permeability constant must decrease from the value measured for a virgin filter. All the different configurations show this same trend. However, when different geometrical configurations of filter elements with the same medium condition are compared, the pressure drop curves are not collinear. This is easily seen by using Darcy's law to calculate the permeability.

FIGURE (1)
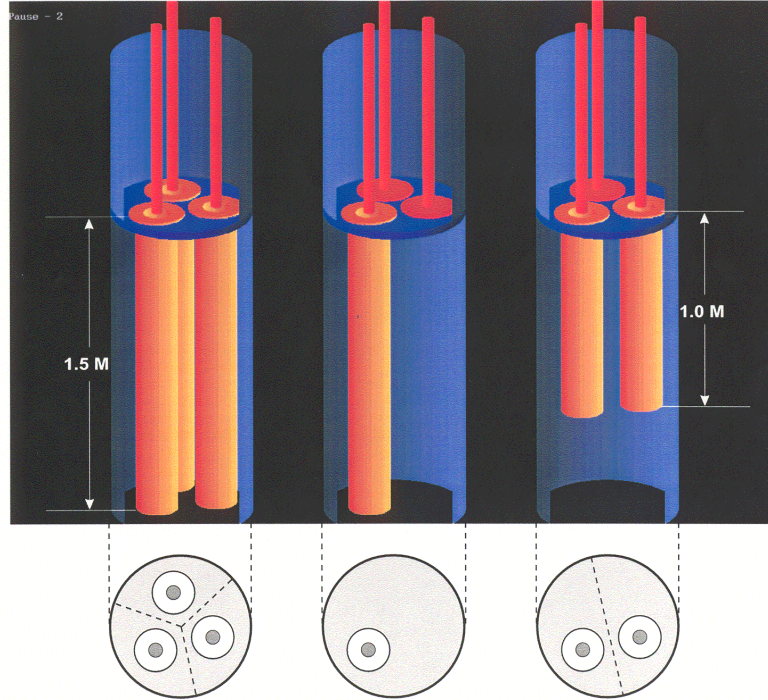
FIGURE (2)

Pressure drop is also dependent on the vessel configuration.

For all the data an effective permeability was calculated using Darcy's law. This model is given as

(1) $$\frac{\Delta P_{sys}}{L_{med}} = -\left(\frac{\mu U_p}{K}\right)$$

Where K = permeability constant

Two effective length scales must be known, or assumed, to effectively use this law in representing the flow through any porous medium. These are the thickness of the porous medium, L_{med}, and the aspect ratio for the porous medium, AR_1. For this particular calculation the medium was assumed to have an effective length of 100 mic. The pores were assumed to be formed by a matrix of squarely packed sintered spherical particles each having a diameter of 10 microns. This gives an aspect ratio of 4.66. An effective pore velocity, U_p, was calculated by multiplying the average face velocity by this aspect ratio. With these parameters a permeability

TABLE (1)

Run	Config.	Filter Cond.	Filter Num	Filter Length (m)	Flow Rate (scfh)	Pressure Drop (inch H$_2$O)	Vessel Pressure (psig)	Vessel Temperature (Deg F)
1	A	Virg	3	1.5	747	0.2747	0.4121	82.51
2	A	Virg	3	1.5	756	0.2747	0.4121	78.01
3	A	Virg	3	1.5	1250	0.4121	0.4121	78.01
4	A	Virg	3	1.5	1256	0.4579	0.4121	81.61
5	A	Virg	3	1.5	1789	0.6410	0.4121	80.71
6	A	Virg	3	1.5	1799	0.5952	0.4121	78.01
7	A	Virg	3	1.5	2201	0.7326	0.5952	79.81
8	A	Virg	3	1.5	3600	1.2821	0.5952	78.91
9	A	Virg	3	1.5	5016	1.8773	0.9615	78.01
10	B	Virg	1	1.5	751	0.5495	0.3663	79.36
11	B	Virg	1	1.5	751	0.5495	0.4121	75.76
12	B	Virg	1	1.5	1240	0.9158	0.3663	79.36
13	B	Virg	1	1.5	1253	0.8700	0.4121	75.76
14	B	Virg	1	1.5	1796	1.3736	0.5495	78.46
15	B	Virg	1	1.5	1804	1.3736	0.4121	75.76
16	B	Virg	1	1.5	2207	1.7857	0.5495	77.56
17	B	Virg	1	1.5	3631	3.3434	0.7784	76.66
18	B	Virg	1	1.5	5000	4.9908	0.9615	74.86
19	B	Virg	1	1.5	751	0.5952	0.3205	75.31
20	B	Virg	1	1.5	756	0.5495	0.3205	71.60
21	B	Virg	1	1.5	1246	0.9158	0.3205	71.60
22	B	Virg	1	1.5	1258	0.9615	0.5037	73.51
23	B	Virg	1	1.5	1799	1.4194	0.5037	73.06
24	B	Virg	1	1.5	1804	1.4652	0.5037	70.70
25	B	Virg	1	1.5	2205	1.8773	0.5037	72.50
26	B	Virg	1	1.5	3609	3.4341	0.6868	71.60
27	B	Virg	1	1.5	5009	5.3114	1.0531	70.70
28	B	Virg	1	1.5	743	0.5952	0.3663	70.70
29	B	Virg	1	1.5	751	0.6410	0.4121	72.50
30	B	Virg	1	1.5	1253	1.0073	0.3663	70.70
31	B	Virg	1	1.5	1256	1.0531	0.4121	71.60
32	B	Virg	1	1.5	1805	1.5568	0.4121	71.60
33	B	Virg	1	1.5	1807	1.5568	0.5495	69.80
34	B	Virg	1	1.5	2199	1.9689	0.5952	71.60
35	B	Virg	1	1.5	3614	3.6172	0.7326	70.70
36	B	Virg	1	1.5	4985	5.6777	1.0989	69.80
37	C	Virg	2	1.0	736	3.522	0.046	109.51
38	C	Virg	2	1.0	747	3.362	0.275	92.52
39	C	Virg	2	1.0	1235	5.599	0.458	91.96
40	C	Virg	2	1.0	1240	5.957	0.412	105.46
41	C	Virg	2	1.0	1784	8.341	0.824	90.16
42	C	Virg	2	1.0	1784	8.700	0.778	101.86
43	C	Virg	2	1.0	2190	10.343	1.328	98.26
44	C	Virg	2	1.0	3627	15.204	3.022	92.86
45	C	Virg	2	1.0	4982	18.928	5.815	87.46

Run	Config.	Filter Cond.	Filter Num	Filter Length (m)	Flow Rate (scfh)	Pressure Drop (inch H$_2$O)	Vessel Pressure (psig)	Vessel Temperature (Deg F)
46	A	Cond	3	1.5	746	0.7326	0.3205	74.41
47	A	Cond	3	1.5	750	0.7326	0.3205	71.60
48	A	Cond	3	1.5	1251	1.1447	0.3205	71.60
49	A	Cond	3	1.5	1253	1.1905	0.5037	73.51
50	A	Cond	3	1.5	1799	1.6026	0.5037	70.70
51	A	Cond	3	1.5	1808	1.6026	0.5037	73.51
52	A	Cond	3	1.5	2198	1.9689	0.5037	72.50
53	A	Cond	3	1.5	3602	3.2967	0.6868	71.60
54	A	Cond	3	1.5	5000	4.6703	1.0531	70.70
55	B	Cond	1	1.5	746	0.9615	0.4121	70.70
56	B	Cond	1	1.5	750	1.0073	0.3205	72.50
57	B	Cond	1	1.5	1249	1.5568	0.4121	70.70
58	B	Cond	1	1.5	1250	1.6026	0.5037	72.50
59	B	Cond	1	1.5	1801	2.3352	0.5952	70.70
60	B	Cond	1	1.5	1805	2.4267	0.5037	71.60
61	B	Cond	1	1.5	2200	2.9762	0.5037	70.70
62	B	Cond	1	1.5	3602	5.2656	0.6868	70.70
63	B	Cond	1	1.5	5005	7.9212	1.0531	69.80
64	B	Cond	1	1.5	745	1.1905	0.3205	72.50
65	B	Cond	1	1.5	747	1.1905	0.3205	71.60
66	B	Cond	1	1.5	1249	1.8773	0.5037	72.50
67	B	Cond	1	1.5	1250	1.9689	0.5037	71.60
68	B	Cond	1	1.5	1798	3.0220	0.5037	72.50
69	B	Cond	1	1.5	1802	3.0220	0.5037	71.60
70	B	Cond	1	1.5	2197	3.8919	0.6868	71.60
71	B	Cond	1	1.5	3600	7.0513	0.8700	71.60
72	B	Cond	1	1.5	4999	10.5311	1.2363	70.70
73	B	Cond	1	1.5	751	1.2821	0.4121	73.96
74	B	Cond	1	1.5	755	1.2363	0.4121	77.56
75	B	Cond	1	1.5	1253	2.2436	0.4121	77.56
76	B	Cond	1	1.5	1256	2.1978	0.4121	73.96
77	B	Cond	1	1.5	1799	3.3425	0.5952	73.96
78	B	Cond	1	1.5	1802	3.4341	0.5952	76.66
79	B	Cond	1	1.5	2201	4.2582	0.5952	75.76
80	B	Cond	1	1.5	3605	7.8755	0.9615	74.86
81	B	Cond	1	1.5	5006	11.7674	1.1447	73.06
82	C	Cond	2	1.0	746	4.067	0.229	107.71
83	C	Cond	2	1.0	786	4.538	0.183	117.61
84	C	Cond	2	1.0	1242	7.402	0.412	107.71
85	C	Cond	2	1.0	1251	7.580	0.550	123.8
86	C	Cond	2	1.0	1795	12.197	1.099	120.31
87	C	Cond	2	1.0	1834	11.339	1.007	105.46
88	C	Cond	2	1.0	2190	15.085	1.465	116.71
89	C	Cond	2	1.0	3578	24.593	3.480	109.51
90	C	Cond	2	1.0	4940	32.484	6.319	102.76
91	D	Cond	384		456000	59.000	150.000	1350
92	D	Cond	128		192000	60.000	150.000	1550

Pressure Drop
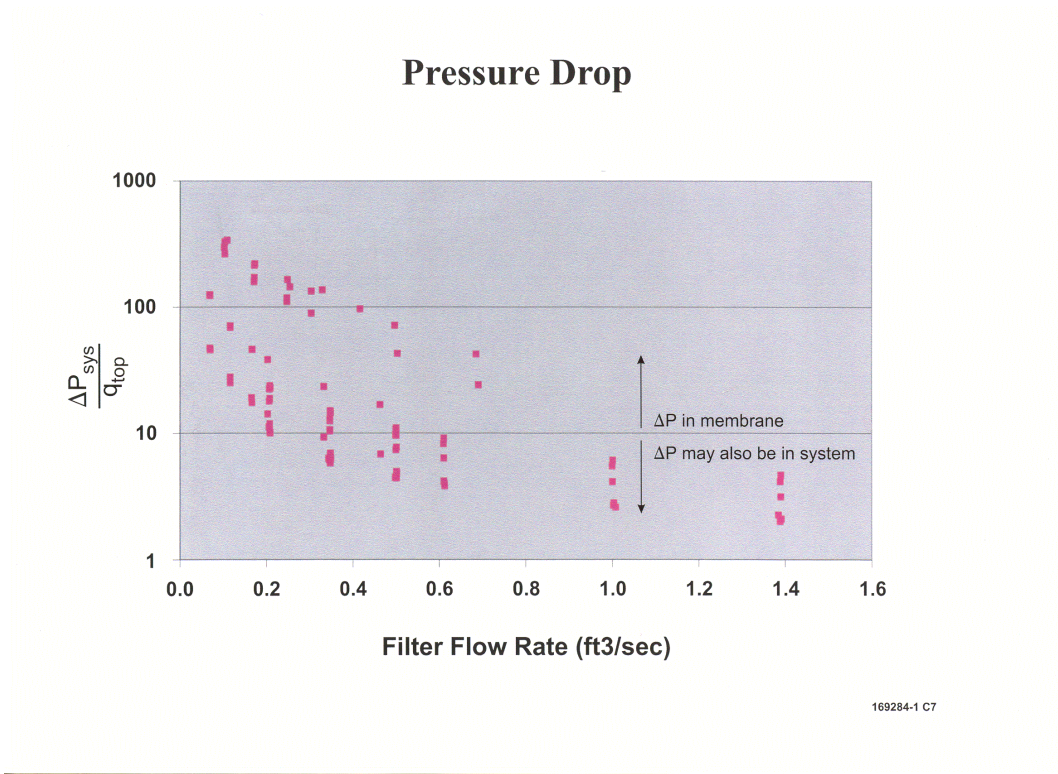

169284-1 C7

FIGURE (3)

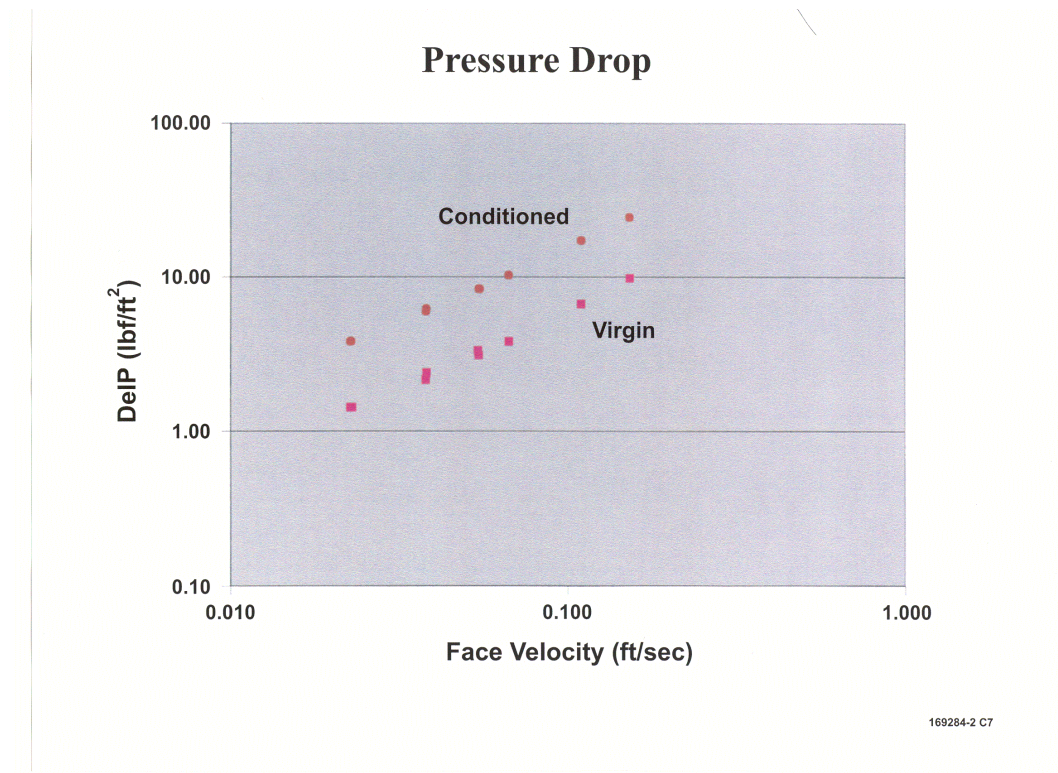## Pressure Drop

169284-2 C7

FIGURE (4)

constant was calculated using Equation (1) and the results are shown in Figure (5). In all cases the calculated permeability for a particular geometrical configuration and filter condition was nearly constant with respect to flow rate. The permeability of the virgin filters was consistently higher than that of the conditioned filters having the same geometric configuration. The permeability for virgin filters with different geometrical configurations differed according to the particular geometry. The same qualitative dependence on configuration geometry is shown for the conditioned filters. The virgin filter data shows a dependence on both the number of filters in the containment vessel and a greater dependence on the length scale of the filter element. The same trends are seen for the entire set of conditioned filter data. From this data alone a preliminary conclusion may be made that the permeability may be a function of the geometrical configuration of the filters within the filter containment vessel. It should be said that there is some question about the condition of the 1.0-meter filter elements. The condition of the filter media was determined largely by inspection. There also may have been some small leaks in the system. So there is sufficient cause to be concerned that the data represented here may not be the whole story. More measurements should be made with a much tighter control over the condition of the filter media.
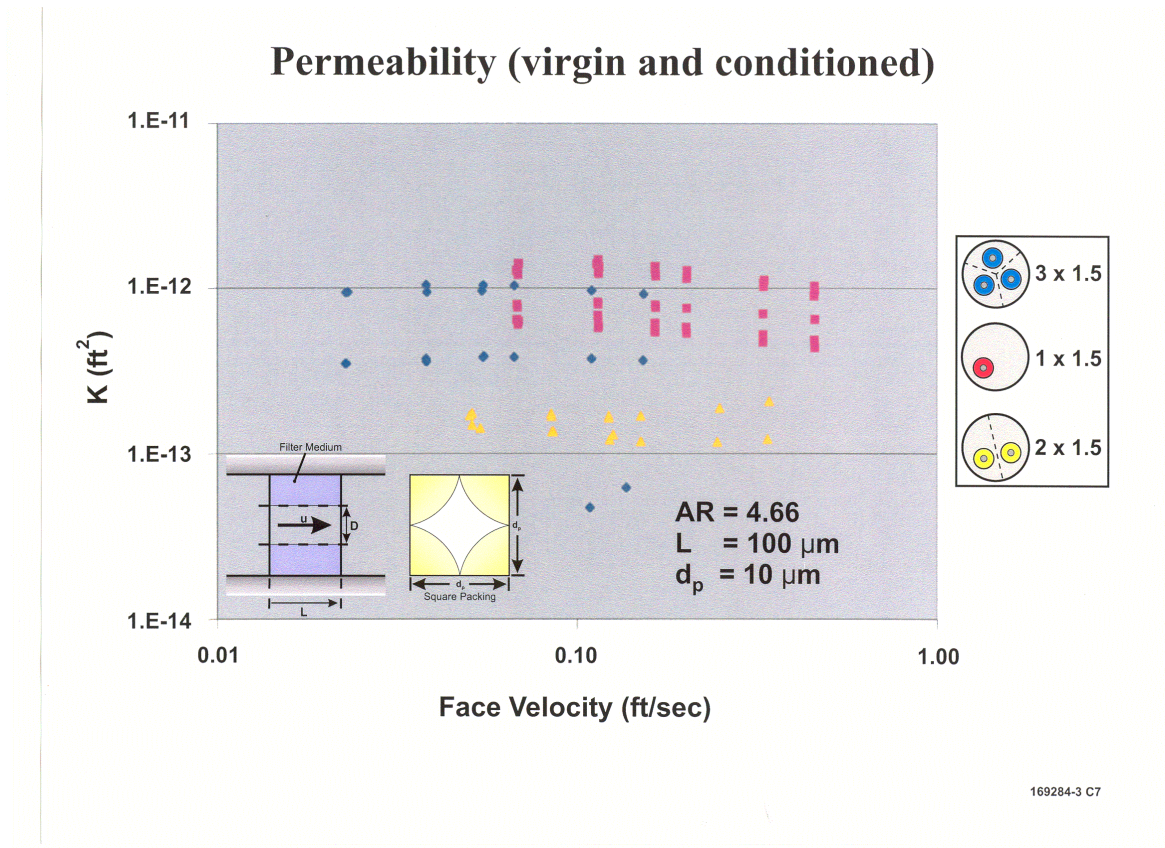

FIGURE (5)

3.0   FILTER AERODYNAMIC PERFORMANCE MODEL

Lumped Analysis

Aerodynamic processes play a vital role in the design and performance of filtration systems. Many types of filters, differing widely in size and configuration have been designed. Close inspection of these systems reveals that many aerodynamic features are common to all systems. In the filter containment vessel the main objective is to reduce the flow velocity and distribute the air evenly to the entire filtration surface. A second consideration, usually never followed, is to maintain as uniform of a flow as is possible in the annulus of the containment vessel with minimal flow recirculation or other parasitic losses. The analysis, which follows, explains why this is so important. This analysis pertains only to filter vessels that are designed with a straight-through flow configuration. While many filtration systems do not follow this basic design, the ideas presented here are easily transferable to those other systems with simple modifications. A number of flow parameters may be defined to facilitate the analysis of the characteristics of the flow inside the filter containment vessel and to allow comparison of the aerodynamic perfor-mance of different filter designs. These parameters include the average velocity of the gas flow in the annulus of the filter containment vessel, U_{ves}, which is the mean velocity across the cross-sectional plane of the filter containment vessel, A_{ves}.

$$(2) \qquad U_{ves} = \frac{\dot{m}}{\rho A_{ves}}$$

Another important reference parameter is the dynamic pressure of the flow in the annulus of the filter containment vessel, q_{ves}, which is given as

$$(3) \qquad q_{ves} = \frac{\rho U_{ves}^2}{2}$$

The equation of state is also needed and is given here as

$$(4) \qquad p = rRT$$

There are two important dimensionless pressure drop parameters that are critical in a successful filter design. These are the "total pressure drop parameter", C_T, which is the ratio of the system pressure drop to the inlet total pressure ($\Delta P_{sys}/P_{ves}$), and the "dynamic pressure drop parameter", C_D, which is a ratio of the system pressure drop to the dynamic pressure of the axial flow in the annulus of the filter containment vessel ($\Delta P_{sys}/q_{ves}$). Combining these pressure drop parameters with the reference quantities defined above gives an equation that is suitable for most filter design purposes. The filter design equation is given as

$$(5) \qquad \frac{\Delta P_{sys}}{P_{ves}} = \frac{\Delta P_{sys}}{q_{ves}} \frac{RT}{2} \left(\frac{\dot{m}}{A_{ves}P} \right)^2$$

For filtration systems that would be used in PFBC and IGCC applications it is generally desirable to keep the total pressure drop parameter to a minimum. The total pressure drop parameter depends on the system operating conditions and so is usually treated as a design constraint. For a given system flow rate the dynamic pressure drop parameter is very important because it represents the total flow resistance introduced into the air stream between the filter inlet and the filter outlet. This term can be thought of as an overall "system drag coefficient", which, for a fixed system flow rate, depends exclusively on the system geometry. If the filtration system experiences a wide range of flow rates then this term will also depend on the flow rate. The remaining terms on the right hand side of Equation (5) form another dimensionless parameter, which is the filter vessel reference velocity. The total pressure drop parameter and the dynamic pressure drop parameter for these experimental runs are listed on Table (2) in the columns marked as Π_1 and Π_2 respectively. The corresponding reference velocity is also shown on Table (2) in the column marked as Π_3. The overall system drag coefficient is noticeably larger than it's companion dimensionless groups and greatly increases with decreasing vessel reference velocity. This is characteristic of all low Reynolds Number flows.

The dynamic pressure drop parameter represents the sum of two separate sources of pressure loss, which are (1) the pressure drop for the flow inside the annulus of the filter containment vessel; and (2) the pressure drop across the filter medium. These are also written in dimensionless form as drag coefficients and are called the "vessel pressure drop parameter", C_V, which is the ratio of the pressure drop inside the containment vessel to the dynamic pressure of the flow inside the containment vessel, ($\Delta P_{ves}/q_{ves}$); the other is the "filter pressure drop parameter", C_F, which is a ratio of the pressure drop across the filter medium to the dynamic pressure of the flow inside the filter containment vessel ($\Delta P_{filt}/q_{ves}$). Thus, the dynamic pressure drop parameter is written as

(6) $$\frac{\Delta P_{sys}}{q_{ves}} = \frac{\Delta P_{ves}}{q_{ves}} + \frac{\Delta P_{filt}}{q_{ves}}$$

Equation (6) is a lumped system performance model that uses drag coefficients to represent the various losses of energy. It splits the overall system drag into two components each of which are taken with respect to the dynamic pressure of the mean flows inside the filter containment vessel. In most filtration system designs aerodynamic performance is measured by taking the ratio of the filter pressure drop to the pressure drop for the entire system. Stated in terms of these drag coefficients this measure of performance is given as

(7) $$\alpha = \frac{C_F}{C_D} < 1$$

The ratio α is always less than 1, but if this ratio is close to one then many filtration engineers assume their design to be good. It means that most of the pressure drop occurs in the filter medium and very little occurs in the filter containment vessel. However, another very important measure of aerodynamic performance, very often overlooked, is the ratio of fluid drag occurring in the annulus of the filter vessel to the fluid drag occurring in the filter medium. This ratio is also written in terms of drag coefficients as

TABLE (2)

Run	Pi1 DelP/Pves	Pi2 DelP/Qves	Pi3 VesRefVel
1	6.56E-04	3453.1	1.90E-07
2	6.56E-04	3343.4	1.96E-07
3	9.84E-04	1834.7	5.36E-07
4	1.09E-03	2032.6	5.38E-07
5	1.53E-03	1400.2	1.09E-06
6	1.42E-03	1279.3	1.11E-06
7	1.73E-03	1042.8	1.66E-06
8	3.02E-03	681.1	4.44E-06
9	4.32E-03	500.8	8.63E-06
10	1.32E-03	6815.0	1.93E-07
11	1.31E-03	6749.0	1.94E-07
12	2.19E-03	4166.2	5.26E-07
13	2.08E-03	3838.6	5.41E-07
14	3.25E-03	2938.0	1.11E-06
15	3.28E-03	2923.7	1.12E-06
16	4.22E-03	2525.1	1.67E-06
17	7.79E-03	1718.0	4.54E-06
18	1.15E-02	1332.1	8.63E-06
19	1.43E-03	7348.7	1.95E-07
20	1.32E-03	6648.6	1.99E-07
21	2.20E-03	4079.1	5.39E-07
22	2.28E-03	4165.7	5.48E-07
23	3.37E-03	3004.5	1.12E-06
24	3.48E-03	3070.6	1.13E-06
25	4.45E-03	2642.4	1.69E-06
26	8.05E-03	1779.8	4.52E-06
27	1.22E-02	1393.5	8.73E-06
28	1.43E-03	7420.5	1.92E-07
29	1.53E-03	7824.9	1.96E-07
30	2.41E-03	4415.7	5.46E-07
31	2.51E-03	4588.3	5.48E-07
32	3.72E-03	3284.3	1.13E-06
33	3.68E-03	3236.5	1.14E-06
34	4.64E-03	2765.1	1.68E-06
35	8.46E-03	1860.8	4.54E-06
36	1.30E-02	1497.0	8.66E-06
37	8.62E-03	49003.6	1.76E-07
38	8.10E-03	43387.0	1.87E-07
39	1.33E-02	26087.9	5.11E-07
40	1.42E-02	28291.7	5.03E-07
41	1.94E-02	18125.4	1.07E-06
42	2.03E-02	19365.9	1.05E-06
43	2.33E-02	14659.0	1.59E-06
44	3.09E-02	7036.3	4.40E-06
45	3.33E-02	3971.6	8.38E-06
46	1.76E-03	9151.3	1.92E-07

Run	Pi1 DelP/Pves	Pi2 DelP/Qves	Pi3 VesRefVel
47	1.76E-03	9006.4	1.95E-07
48	2.75E-03	5058.0	5.44E-07
49	2.82E-03	5199.1	5.43E-07
50	3.80E-03	3377.3	1.13E-06
51	3.80E-03	3361.4	1.13E-06
52	4.67E-03	2789.0	1.68E-06
53	7.73E-03	1715.3	4.51E-06
54	1.07E-02	1229.7	8.70E-06
55	2.30E-03	11854.9	1.94E-07
56	2.42E-03	12404.4	1.95E-07
57	3.72E-03	6847.6	5.43E-07
58	3.80E-03	7019.1	5.42E-07
59	5.51E-03	4880.8	1.13E-06
60	5.76E-03	5088.6	1.13E-06
61	7.06E-03	4193.9	1.68E-06
62	1.23E-02	2735.0	4.51E-06
63	1.81E-02	2077.9	8.73E-06
64	2.86E-03	14857.9	1.92E-07
65	2.86E-03	14753.4	1.94E-07
66	4.45E-03	8235.4	5.41E-07
67	4.67E-03	8608.8	5.43E-07
68	7.17E-03	6397.2	1.12E-06
69	7.17E-03	6358.1	1.13E-06
70	9.12E-03	5443.1	1.68E-06
71	1.63E-02	3629.6	4.50E-06
72	2.38E-02	2742.0	8.69E-06
73	3.06E-03	15693.9	1.95E-07
74	2.95E-03	15074.4	1.96E-07
75	5.36E-03	9932.4	5.39E-07
76	5.25E-03	9618.3	5.45E-07
77	7.88E-03	7044.8	1.12E-06
78	8.10E-03	7250.3	1.12E-06
79	1.00E-02	6016.0	1.67E-06
80	1.81E-02	4043.7	4.49E-06
81	2.68E-02	3086.7	8.68E-06
82	9.83E-03	54235.3	1.81E-07
83	1.10E-02	55636.5	1.98E-07
84	1.77E-02	35181.6	5.02E-07
85	1.79E-02	36191.7	4.95E-07
86	2.78E-02	27137.4	1.03E-06
87	2.60E-02	23684.6	1.10E-06
88	3.37E-02	21899.8	1.54E-06
89	4.88E-02	11745.1	4.16E-06
90	5.58E-02	6955.7	8.02E-06
91	1.29E-02	16102.1	8.03E-07
92	1.31E-02	25467.1	5.16E-07

$$(8) \qquad \beta = \frac{C_V}{C_F}$$

β represents a ratio of drag coefficients, not a ratio of pressure drops. The annulus of the filter vessel can have a high value of β even with a very small pressure drop because the dynamic pressure in some parts of the annulus is vanishingly small. Using the performance parameters expressed in Equations (7) and (8), Equation (6) is rewritten as

$$(9) \qquad \alpha = \frac{1}{(\beta + 1)}$$

The relationship between α and β is shown in Figure (6). It is explicit that β be small for filtration systems having a value of α that approaches one. However, as β increases, α decreases and approaches zero for high values of β. As α decreases a condition can occur where most of the fluid dynamic drag is in the annulus of the filter containment vessel.

The values of these various performance parameters may be related to the flow inside the filter medium by defining some additional reference quantities. A coefficient of drag for the filter medium, C_f, is defined as the ratio of the pressure drop across the medium to the dynamic pressure of the flow in the individual pores of the filter medium, $(\Delta P_{filt}/q_p)$. This coefficient is calculated using the velocity of the flow within a single pore of the filter medium as the reference velocity. It is given as

$$(10) \qquad U_p = \frac{\dot{m}_p}{\rho A_p}$$

The dynamic pressure for the flow in a single pore of the filter medium is given as

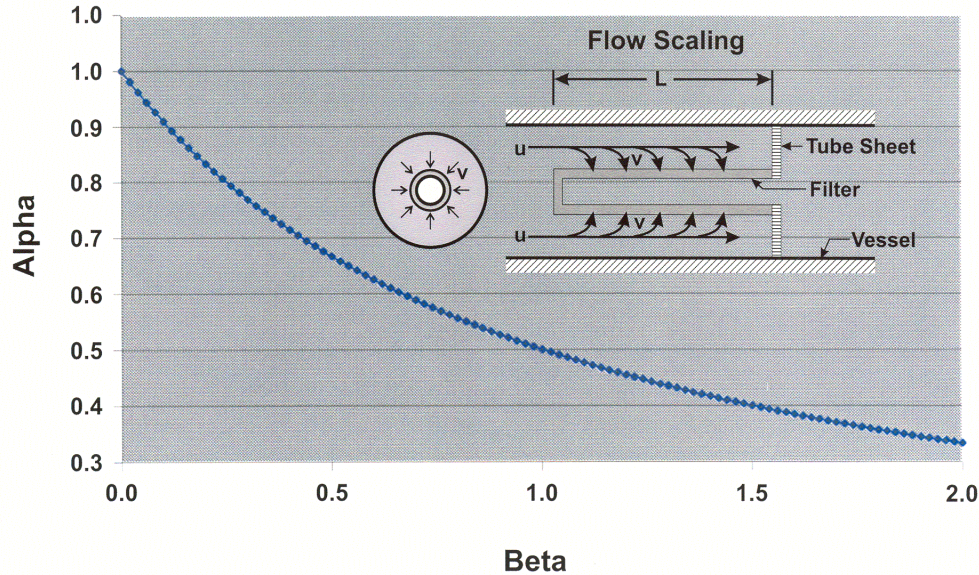$$(11) \qquad q_p = \frac{\rho U_p^2}{2}$$

To relate this flow to the flow in the annulus of the filter containment vessel the following area ratios must be defined.

$$(12) \qquad AR_1 = \frac{A_{tot}}{A_{ves}} > 1$$

and

$$(13) \qquad AR_2 = \frac{A_a}{A_p} > 1$$

Filter Aerodynamic Performance

FIGURE (6)

The aspect ratio AR_1 represents the diffusive flow in the annulus of the filter containment vessel. It is the ratio of the total surface area, A_{tot}, of all the filters in the vessel to the cross-sectional reference area of the filter containment vessel. Usually this aspect ratio is greater than 1. A second aspect ratio, AR_2, represents the contraction of the flow as it passes from the average face velocity taken over an approach area, A_a, to the interstitial velocity of the flow in a single pore of the filter medium. The approach area is related to the total filter surface area by

(14) $A_{tot} = nA_a$

Where n = the total number of pores in the filter medium.

In optimizing the design of any particular filtration system the assumption is often made that the face velocity is uniform over the entire extent of the filter surface area. With this assumption the conservation of mass may be written as

(15) $U_{ves}A_{ves} = nU_pA_p$

Equations (10) through (15) are then combined to relate C_F to C_f. This relationship is given as

(16) $\quad C_F = C_f \left(\dfrac{AR_1}{AR_2} \right)^2$

The essential difference between C_F and C_f is that they are based on different dynamic pressures. In order to achieve good aerodynamic performance, i.e. α near 1, the typical filtration system designer will attempt to minimize β. He does this by following Equation (8) and increases C_F to as high a value as is possible. Equation (16) shows that C_F may be increased by making the ratio of the aspect ratios as large as possible. The aspect ratio of the filter medium, AR_2, is a geometrical property of the filter medium that is set by the manufacturing process and therefore cannot be changed by the system designer. So, larger values of C_F are achieved by maximizing AR_1. This is done by making the total filter surface area as large as possible. This practice brings about a design dilemma. AR_1 can be maximized only at the expense of reducing the cross sectional area open to flow in the annulus of the filter containment vessel. By reducing this area the dynamic pressure of the flow at the entrance of the vessel is increased. The annulus thus experiences an extended range in the Reynolds number of this flow as it passes from a relatively large value at vessel inlet to a vanishingly small value at the end of the vessel. Extending the range of the Reynolds number of the flow in the annulus greatly effects the flow in the filter media. This gives rise to the variations in the permeability within the filter vessel. Ultimately, the use of Equation (15) for a detailed system design should be avoided. This is because U_p cannot be considered to be constant, but must adjust itself to be commensurate with the Reynolds number of the mean flow in the annulus of the filter containment vessel. The distributed analysis, which follows, shows why.

Distributed Analysis

The drag coefficients C_V and C_F used in the calculation of the aerodynamic performance parameters α and β were derived by considering only the average fluid drag which was integrated over the entire system. Examination of these parameters may also be done in various locations inside the filter containment vessel. In this case the variations of these parameters shows that a situation of uneven flow distribution is a condition which necessarily exists in all systems that are designed in a straight-through flow configuration. The distributed analysis shows that the assumption of uniform face velocity made in writing Equation (15) cannot be accurate and thus permeability must be a variable which depends on the mean flows in the vessel.

To facilitate in deriving the aerodynamic performance criterion for the distributed analysis the filtration system is divided into the several finite sections that are shown in Figure (7). New reference flow parameters are defined which pertain to a single finite section of the annulus only. These parameters are considered constant in a single section but are allowed to change along the annulus for each section. The average flow in the annulus of the vessel for any particular finite section is given as

(17) $\quad U_v = \dfrac{\dot{m}_v}{\rho A_v} = \dfrac{Q_v}{A_v}$

Filter Performance Depends on Mean Flows

Inlet at bottom
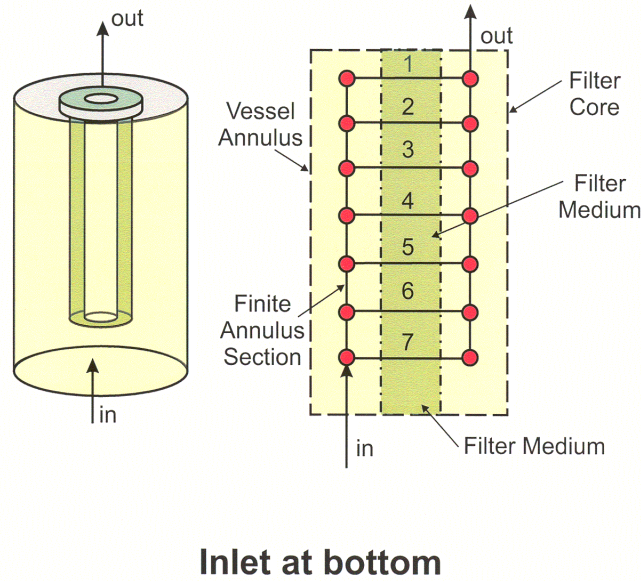
169284-7 C7

FIGURE (7)

The dynamic pressure for this flow is given as

$$(18) \qquad q_v = \frac{\rho U_v^2}{2}$$

Equations (17) and (18) are analogous to Equations (2) and (3); but they apply only to a section of the annulus of the filter containment vessel. Again, two important dimensionless pressure drop parameters are related using the newly defined reference flow parameters. These are C_t', which is the ratio of the pressure drop in the annulus of the finite section plus the pressure drop in the filter medium to the absolute pressure in the annulus of the vessel at that point, $(\Delta P_{vf}/P_v)$, and also, C_d', which is the ratio of the same pressure drop to the dynamic pressure in the annulus at that section, $(\Delta P_{vf}/q_v)$. Using Equations (17) and (18) to combine these reference flow parameters gives

$$(19) \qquad \frac{\Delta P_{vf}}{P_v} = \frac{\Delta P_{vf}}{q_v} \frac{RT}{2} \left(\frac{\dot{m}}{A_v P} \right)^2$$

Equation (19) is the analogue to Equation (5) and so the term $(\Delta P_{vf}/q_v)$ refers to a drag coefficient, C_d', which represents the sum of the fluid drag for the flow as it passes through both the finite section of the annulus and also the filter medium at that point. As was done in Equation (6) this drag coefficient may be separated into it's parts $(\Delta P_v/q_v)$, and $(\Delta P_f/q_v)$ which are C_v', and C_f' respectfully. They are written as

$$(20) \quad \frac{\Delta P_{vf}}{q_v} = \frac{\Delta P_v}{q_v} + \frac{\Delta P_f}{q_v}$$

Equation (20) is a system performance model, analogous to Equation (6), but applies only to the finite axial section of the annulus of the filter vessel, which has been coupled to the filter medium at that point. It is written in this way so that the effects of a diminishing velocity in the annulus of the containment vessel may be examined. Using these drag coefficients to define local aerodynamic performance parameters which are given as

$$(21) \quad \alpha' = \frac{C_f'}{C_d'}$$

and

$$(22) \quad \beta' = \frac{C_v'}{C_f'}$$

Equations (20), (21), and (22) are written as

$$(23) \quad \alpha' = \frac{1}{(\beta'+1)}$$

Equation (23) can now be used to compare the local filter performance between any two axial sections of the filter containment vessel. By inspection Equation (23) is identical to Equation (9) and so it follows the same behavior shown in Figure (6).

A complete analysis of β' is accomplished by relating C_f to C_f'. Noticing that like Equation (16), the two drag coefficients are related by a constant area ratio k. This ratio will be a function of the number of the finite axial divisions shown in Figure (7), but it cannot change with each successive section along the axis of the filter containment vessel. The local aerodynamic performance parameter is rewritten as

$$(23) \quad \beta' = k \frac{C_v'}{C_f}$$

For low Reynolds number flows both C_v' and C_f may be taken as reciprocal functions of the Reynolds number, so the performance parameter may be written

$$(24) \quad \beta' \sim k\left(\frac{Re_f}{Re_v}\right) = k\left(\frac{U_p D_p}{U_v D_v}\right)$$

Using Equations (12), (13), and (14) to relate the ratio of the diameters, (D_p/D_v), to the cross-sectional areas open to the flow the performance parameter is written as

$$(25) \quad \beta' \sim k\left[\frac{U_p}{U_v}\left(\frac{AR_1}{AR_2}\frac{1}{n}\right)^{\frac{1}{2}}\right]$$

Equation (25) shows that the local filter performance parameter β' depends on a local area ratio parameter, k, which is a function of the finite axial divisions of the system, a global area ratio parameter (AR_1/AR_2), and the total number of pores in the filter media. Since all of these area ratios are the same for each axial section, the local variation of β' depends only on the ratio of the pore velocity to the annulus velocity. If the velocity of the flow in the pores of the filter medium maintains a finite value, then, as U_v tends to 0, β' must increase. This will in-turn cause α' to decrease. Thus U_p must continually adjust to this and so it cannot be constant. For low Reynolds number flows in the annulus the aerodynamic performance of the system must diminish with each additional axial section.

4.0   ANALYSIS OF THE NETL EXPERIMENTAL RUNS

The division of the three laboratory configurations shown in Figure (2) into separate finite annular sections is shown in Figure (8). For each region the pertinent geometrical reference conditions that effect the pressure drop calculation and the dynamic pressure of the flows in the various sections are shown on Table (3). For each section an initial flow rate is assumed and the stagnation pressure drop is calculated using models for the drag coefficients C_v' and C_f. The flow rate in each element is then increased or decreased until the stagnation pressure at every node in the network balances. The drag coefficient models that are used in the calculation have been fit to match the experimental data. The results of the network model in predicting the pressure drop performance of the three experimental configurations is shown in Figure (9).

5.0   ANALYSIS OF INDUSTRIAL SCALE THREE-TIER SYSTEM

An analysis was done of a larger scale one-column, the three-tier HGCU system. A schematic diagram of this system and the companion network flow model is shown in Figures (10) and (11). The operating conditions for these calculations were taken from reference 5. For this particular calculation it is presumed that the fluid entering the filter containment vessel is an axial flow coming from the top of the vessel.
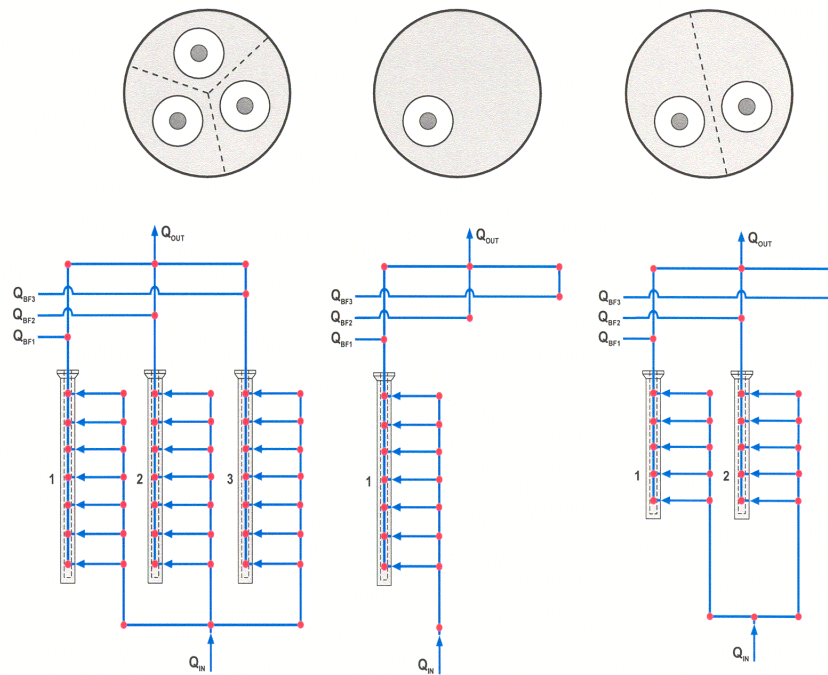
FIGURE (8)

To show the effect that the various drag coefficients have on the distribution of the flow within the filter vessel an average value of the aerodynamic performance parameter β' was assumed to be a constant throughout the entire vessel. While this is generally not the case, as was shown in section 3.0, the assumption does serve to illustrate the importance of this parameter in determining the aerodynamic performance of the filter vessel. For a given value of β' the pressure balance model was run and the integrated flow collected from every filter in each tier of the filter vessel was calculated. The aerodynamic performance parameter was successively increased with the completion of each additional run and the entire calculation was repeated. This was done for an extended range of the aerodynamic performance parameter. The results are shown in Figure (12). The variation of the aerodynamic performance parameter is shown on the abscissa. It was run from the exceedingly small value of 10^{-8} and increased to the value of 10^{-1}. The ordinance shows the resulting cumulative flow rate coming from each tier. In this particular design there are 38 filters on the top and middle tiers and 52 filters on the bottom tier giving a total of 128 filters in the system. When the flow coupling parameter is low the flow is evenly distributed among all the filter elements so that the cumulative normalized flow rate into each of the upper two tiers would be 38/128, or approximately 30 percent. The cumulative flow into the bottom tier would be 52/128 or approximately 40 percent. The very low value of β' is analogous to neglecting frictional

TABLE (3)

	Conf A	Conf B	Conf C	Ext	Med	Int
Nfilt	3	1	2			
Nsec	6	6	4			
Nmed	7	7	5			
Vessel Dimensions						
Lves (ft)	4.9180	4.9180	3.2787			
Dves (ft)	0.6667	0.6667	0.6667			
Aves (ft^2)	0.3491	0.3491	0.3491			
Cves (ft)	2.0944	2.0944	2.0944			
Lsec (ft)	0.8197	0.8197	0.8197	*		*
Lmed (ft)	0.7026	0.7026	0.6557			
Filter Exterior Dimensions - (Cross-Section)						
DODfilt (ft)	0.1969	0.1969	0.1969			
AODfilt (ft^2)	0.0304	0.0304	0.0304			
CODfilt (ft)	0.6184	0.6184	0.6184			
Filter Interior Dimensions -(Cross-Section)						
DIDfilt (ft)	0.1312	0.1312	0.1312			*
AIDfilt (ft^2)	0.0135	0.0135	0.0135			*
CIDfilt (ft)	0.4123	0.4123	0.4123			*
Annulus Dimensions - (Cross-Section)						
Ablock (ft^2)	0.0913	0.0304	0.0609			
Aopen (ft^2)	0.2578	0.3186	0.2882			
Pwet (ft)	3.9497	2.7128	3.3312			
Dhyd (ft)	0.2610	0.4698	0.3461			
Anulus Section						
DsecEF (ft)	0.2610	0.4698	0.3461	*		
AsecEF (ft^2)	0.0859	0.3186	0.1441	*		
Psec (ft)	1.3166	2.7128	1.6656	*		
Medium Section						
Aeff (ft^2)	0.4345	0.4345	0.4055		*	
Leff (ft^2)	0.0656	0.0656	0.0656		*	
Peff (ft)	2.6420	2.6420	2.5483		*	
Deff (ft)	0.6578	0.6578	0.6365		*	
Total Aspect Ratio						
AF (ft^2)	3.0414	3.0414	2.0276			
AFtot (ft^2)	9.1243	3.0414	4.0552			
AR tot	35.3979	9.5453	14.0710			
Anulus Aspect Ratio						
ARsec	5.0568	1.3636	2.8142			
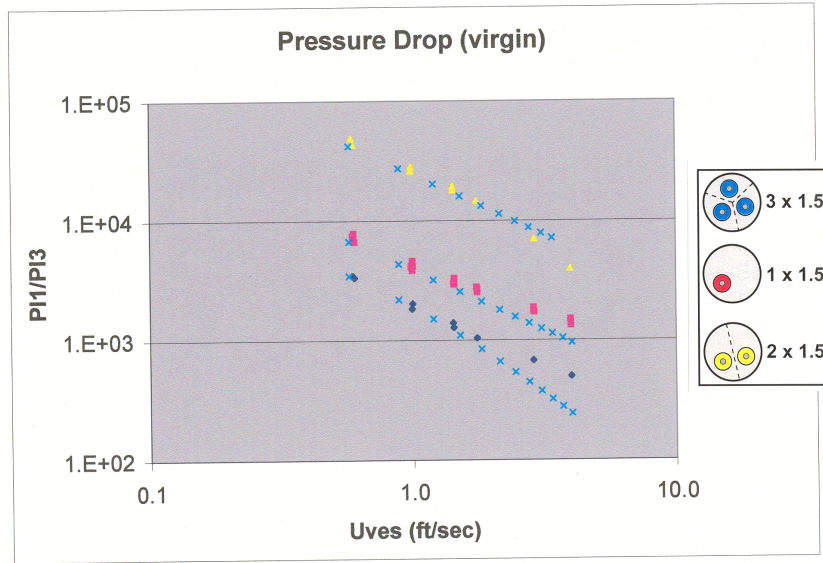
FIGURE (9)

FIGURE (10)

FIGURE (11)

Flow Coupling

Fraction of Flow Entering Tiers (y-axis)

- Tier 1
- Tier 2
- Tier 3
- $\dfrac{52}{128}$
- $\dfrac{38}{128}$

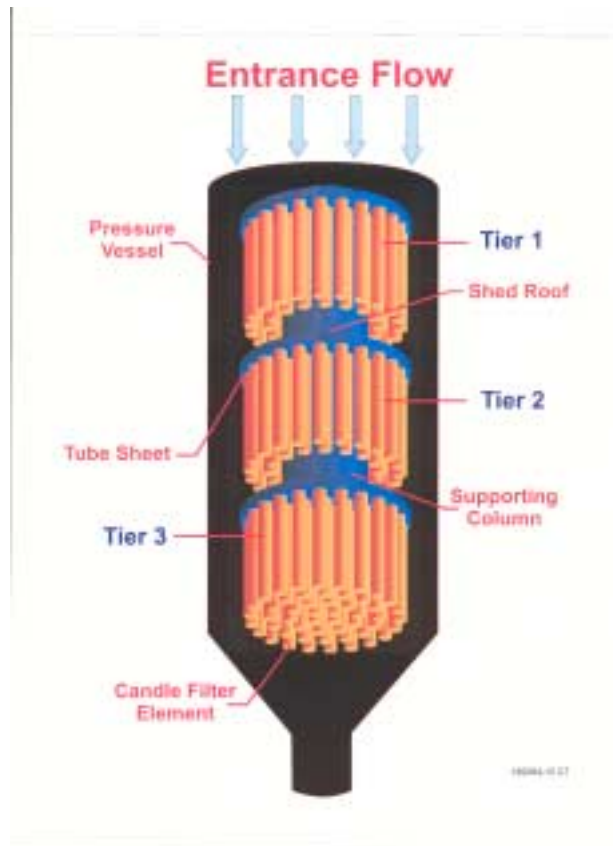x-axis: 1.E-08, 1.E-07, 1.E-06, 1.E-05, 1.E-04, 1.E-03, 1.E-02, 1.E-01
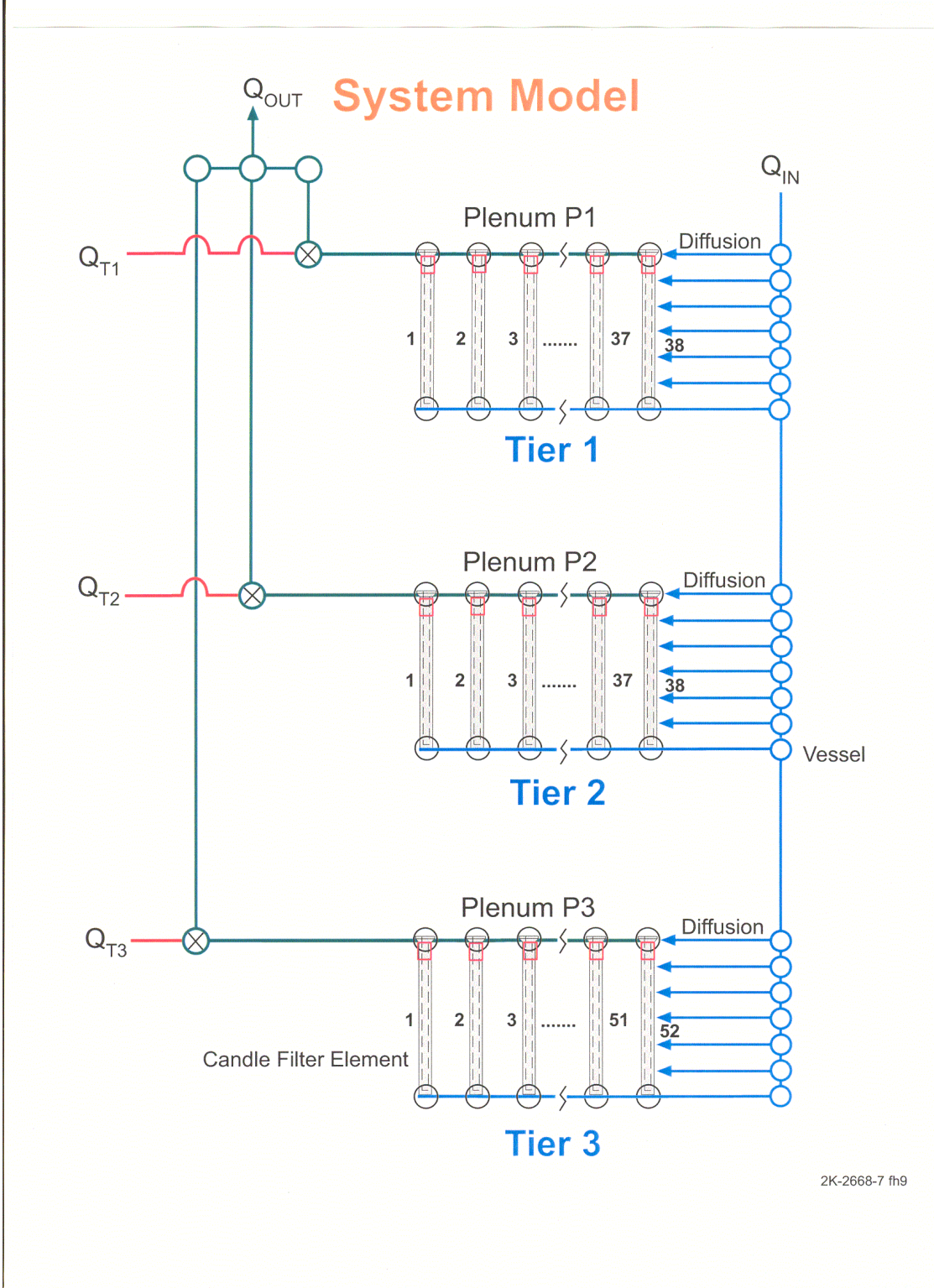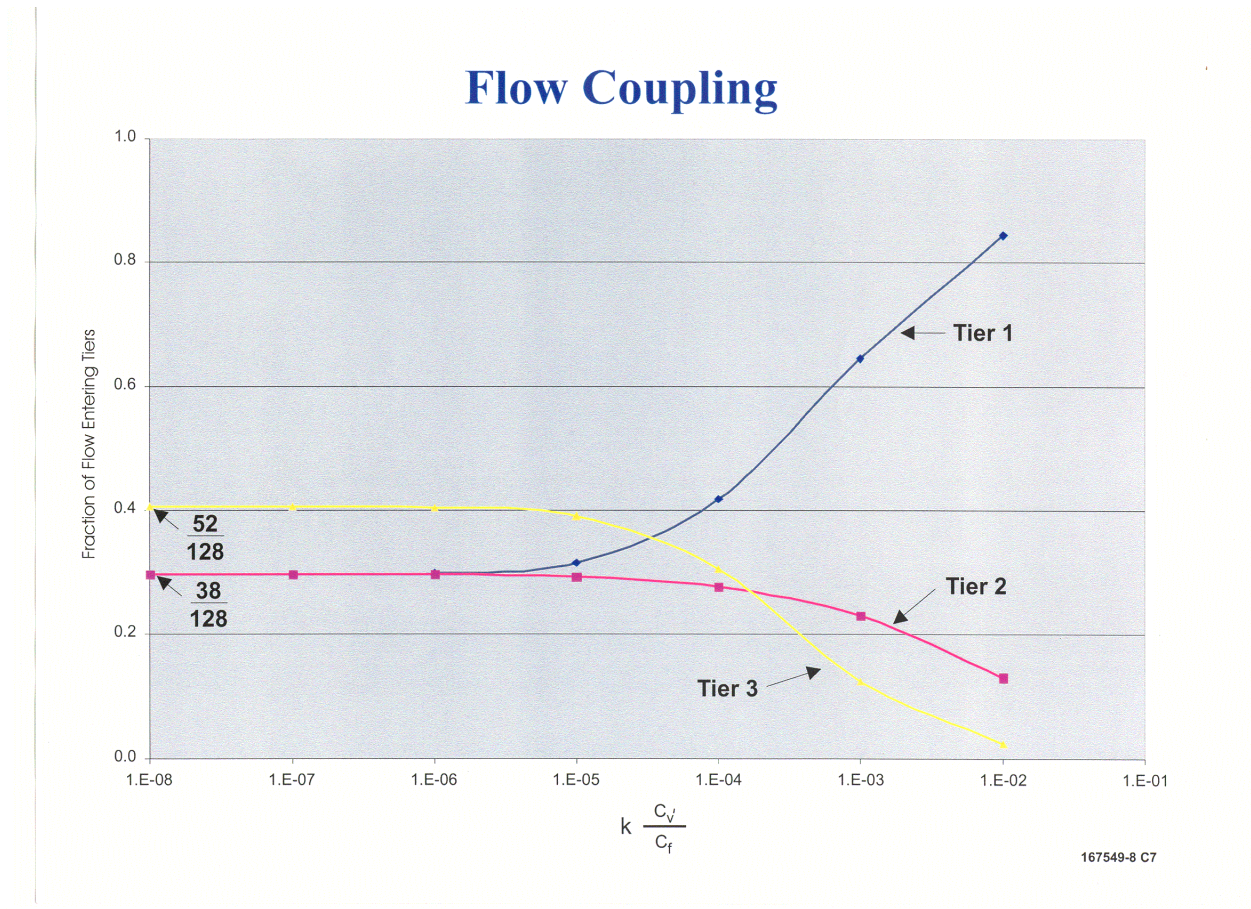
$$k\ \frac{C_v{}'}{C_f}$$

167549-8 C7

FIGURE (12)

effects in the annulus of the filter containment vessel. However, as the ratio of this flow coupling parameter increases a deviation in this even distribution of flow is noticed. The deviation starts to occur when the flow coupling parameter is still very small, only one part in ten thousand. The deviation continues to increase with β' until more than eighty percent of the flow enters the top tier with almost no flow entering the bottom tier even though the bottom tier has more filter elements than the top and middle tiers.

6.0 CONCLUSIONS

Preliminary conclusions are that the normal assumption that all the filter elements of a particular hot gas filtration system have a uniform face velocity does not include the coupling effects of the mean flows in the filter containment vessel. The flow of gas through the filtration medium depends on the characteristics of the mean flows in the containment vessel. Very small changes in the drag of the fluid in the annulus of the containment vessel greatly effect the flow distribution of flow within the filter vessel.

7.0   REFERENCES

1. Dittler, A., M. V. Ferer, P. Mathur, P. Djuranovic, G. Kasper, and D. H. Smith. <u>Patchy Cleaning of Rigid Gas Filters – Transient Regeneration Phenomena Comparison of Modeling to Experiment</u>. Morgantown, WV. U.S. Department of Energy.

2. Fitch, E. C. Copyright 1979. <u>An Encyclopedia of Fluid Contamination Control for Hydraulic Systems</u>. Stillwater, Oklahoma: Hemisphere Publishing Corporation.

3. Geldart, D. Copyright 1986. <u>Gas Fluidization Technology</u>. University of Bradford, UK: John Wiley & Sons.

4. Howard, J. H. G., A. B. Thornton-Trump, and H. J. Henseler, Performance and Flow Regimes for Annular Diffusers, ASME Paper 67-WA/FE-21 (A68-11861).

5. Isaksson, J., R. A. Dennis, and R. A. Brown. 1995. <u>Testing of the Westinghouse Hot Gas Filter at Ahlstrom Pyropower Corporation</u>. Pittsburgh, PA: Westinghouse Science and Technology Center.

6. Kline, S. J., D. E. Abbott, and R. W. Fox, Optimum Design of Straight-Walled Diffusers, *J. Basic Eng.*, vol. 81, pp. 321-331, 1959.

7. McDonald, A. T., and R. W. Fox, An Experimental Investigation of Incompressible Flow in Conical Diffusers, *Int. J. Mech. Sci.*, vol. 8, pp. 125-139, 1966.

8. Mudd, M. J., and J. D. Hoffman. 1995. <u>Operating Experience from the Tidd PFBC Hot Gas Clean Up Program</u>. Columbus, Ohio: American Electric Power Service Corporation.

9. Shames, Irving H. 1962. <u>Mechanics of Fluids</u>. State University of New York at Buffalo: McGraw-Hill Book Company.

10. Smith, D. H., V. Powell, G. Ahmadi, and E. Ibrahim. 1997. <u>Analysis of Operational Filtration Data, Part I. Ideal Candle Filter Behavior</u>. Morgantown, WV: U.S. Department of Energy.

11. Smith, D. H., V. Powell, and G. Ahmadi. 1997. <u>Analysis of Operational Filtration Data, Part II. Incomplete Cleaning of Candle Filters</u>. Morgantown, WV: U.S. Department of Energy.

12. Smith, D. H., V. Powell, G. Ahmadi, and M. Ferer. 1998. <u>Analysis of Operational Filtration Data, Part III. Re-entrainment and Incomplete Cleaning of Dust Cake</u>. Morgantown, WV. Elsevier Science, Inc.

13. Tennekes, H., and J. L. Lumley. Copyright 1972. <u>A First Course in Turbulence</u>. Cambridge, Massachusetts, and London, England: The MIT Press.

14. White, Frank M. Copyright 1974. <u>Viscous Fluid Flow</u>. University of Rhode Island, Kingston, Rhode Island: McGraw-Hill Book Company.

15. Zeh, C. M., T.-K. Chiang, and W. J. Ayers. May 1990. <u>Evaluating the Performance of Ceramic Candle Filters in a Hot Particulate-Laden Stream</u>. Morgantown, WV: U.S. Department of Energy.